Photovoltaic effect in multiphase Bi-Mn-O thin films

J. P. Chakrabartty,[1] R. Nechache,[2,4] C. Harnagea,[1] and F. Rosei[1,3,*]

[1]*Centre Énergie, Matériaux et Télécommunications, Institut national de la recherche scientifique (INRS), 1650 boulevard Lionel-Boulet, Varennes, Québec J3X 1S2, Canada*

[2]*NAST Center & Department of Chemical Science and Technology, University of Rome Tor Vergata Via della Ricerca Scientifica 1, 00133 Rome, Italy*

[3]*Center for Self-Assembled Chemical Structures (CSACS), McGill University, H3A, Montreal, Canada*

[4]*nechache@emt.inrs.ca*

[*]*rosei@emt.inrs.ca*

Abstract: We report an external solar power conversion efficiency of ~0.1% in Bi-Mn-O thin films grown onto (111) oriented Niobium doped $SrTiO_3$ (STO) single crystal substrate by pulse laser deposition (PLD). The films contain $BiMnO_3$ (BMO) and Mn_3O_4 (MO) phases, which both grow epitaxially. The growth conditions were tailored to obtain films with different Bi/Mn ratios. The films were subsequently illuminated under a sun simulator (AM 1.5 G). We find that the Bi/Mn ratio in the film affects the magnitude of the photo induced voltage and photocurrent and therefore the photovoltaic conversion efficiency. Specifically, a higher Bi/Mn ratio (towards unity) in the film increases the power conversion efficiency. This effect is described in terms of a more favorable energy band alignment of the film/substrate hetero-structure junction, which controls photo carrier separation.

OCIS codes: (040.5350) Photovoltaic; (160.2260) Ferroelectrics; (240.0310) Thin films; (310.5448) Polarization, other optical properties; (310.6845) Thin film devices and applications.

References and links

1. S. M. Sze, *Semiconductor Devices: Physics and Technology* (Wiley, 2002).
2. F. Zheng, J. Xu, L. Fang, M. R. Shen, and Z. L. Wu, "Separation of the Schottky barrier and polarization effects on the photocurrent of Pt sandwiched $Pb(Zr_{0.20}Ti_{0.80})O_3$ films," Appl. Phys. Lett. **93**(17), 172101 (2008).
3. W. Ji, K. Yao, and Y. C. Liang, "Bulk photovoltaic effect at visible wavelength in epitaxial ferroelectric $BiFeO_3$ thin films," Adv. Mater. **22**(15), 1763–1766 (2010).
4. Z. Luo, J. H. Hao, and J. Gao, "Rectifying characteristics and transport behavior of $SrTiO_{3-\delta}$(110)/p-Si (100) heterojunctions," Appl. Phys. Lett. **91**(6), 062105 (2007).
5. Y. S. Xiao, X. P. Zhang, and Y. G. Zhao, "Negative differential resistance in$La_{0.67}Ca_{0.33}MnO_{3-\delta}$/Nb–$SrTiO_3$ p-n junction," Appl. Phys. Lett. **90**(1), 013509 (2007).
6. S. M. Guo, Y. G. Zhao, C. M. Xiong, and P. L. Lang, "Rectifying I-V characteristic of $LiNbO_3$/Nb-doped$SrTiO_3$ heterojunction," Appl. Phys. Lett. **89**(22), 223506 (2006).
7. M. Glass, D. Von der Linde, and T. J. Negran, "High-voltage bulk photovoltaic effect and the photorefractive process in $LiNbO_3$," Appl. Phys. Lett. **25**(4), 233–235 (1974).
8. Y. S. Yang, S. L. Lee, S. Yi, B. G. Chae, S. H. Lee, H. J. Joo, and M. S. Jang, "Schottky barrier effects in the photocurrent of sol–gel derived lead zirconate titanate thin film capacitors," Appl. Phys. Lett. **76**(6), 774 (2000).
9. L. Pintilie, I. Vrejoiu, G. Le Rhun, and M. Alexe, "Short-circuit photocurrent in epitaxial lead zirconate-titanate thin films," J. Appl. Phys. **101**(6), 064109 (2007).
10. S. Y. Yang, L. W. Martin, S. J. Byrnes, T. E. Conry, S. R. Basu, D. Paran, L. Reichertz, J. Ihlefeld, C. Adamo, A. Melville, Y. Chu, C. Yang, J. L. Musfeldt, D. G. Schlom, J. W. Ager III, and R. Ramesh, "Photovoltaic effects in $BiFeO_3$," Appl. Phys. Lett. **95**(6), 062909 (2009).
11. H. Schmid, "Multi-ferroic magnetoelectrics," Ferroelectrics **162**(1), 317–338 (1994).
12. H. R. Condit and F. Grum, "Spectral energy distribution of daylight," J. Opt. Soc. Am. **54**(7), 937–944 (1964).
13. S. Y. Yang, J. Seidel, S. J. Byrnes, P. Shafer, C.-H. Yang, M. D. Rossell, P. Yu, Y. H. Chu, J. F. Scott, J. W. Ager 3rd, L. W. Martin, and R. Ramesh, "Above-bandgap voltages from ferroelectric photovoltaic devices," Nat. Nanotechnol. **5**(2), 143–147 (2010).
14. R. Guo, L. You, L. Chen, D. Wu, and J. Wang, "Photovoltaic property of $BiFeO_3$ thin films with 109° domains," Appl. Phys. Lett. **99**(12), 122902 (2011).

#195123 - $15.00 USD Received 2 Aug 2013; revised 25 Nov 2013; accepted 25 Nov 2013; published 5 Dec 2013

15. N. A. Hill and K. M. Rabe, "First-principles investigation of ferromagnetism and ferroelectricity in bismuth manganite," Phys. Rev. B **59**(13), 8759–8769 (1999).
16. J. Y. Son and Y. H. Shin, "Multiferroic $BiMnO_3$ thin films with double $SrTiO_3$ buffer layers," Appl. Phys. Lett. **93**(6), 062902 (2008).
17. W. Eerenstein, F. D. Morrison, J. F. Scott, and N. D. Mathur, "Growth of highly resistive $BiMnO_3$ films," Appl. Phys. Lett. **87**(10), 101906 (2005).
18. H. Chiba, T. Atou, and Y. Syono, "Magnetic and electrical properties of $Bi_{1-x}SrxMnO_3$: hole-doping effect on ferromagnetic perovskite $BiMnO_3$," J. Solid State Chem. **132**(1), 139–143 (1997).
19. A. F. Moreira dos Santos, A. K. Cheetham, W. Tian, X. Pan, Y. Jia, N. J. Murphy, J. Lettieri, and D. G. Schlom, "Epitaxial growth and properties of metastable $BiMnO_3$ thin films," Appl. Phys. Lett. **84**(1), 91–93 (2004).
20. H. Béa, M. Bibes, A. Barthélémy, K. Bouzehouane, E. Jacquet, A. Khodan, J.-P. Contour, S. Fusil, F. Wyczisk, A. Forget, D. Lebeugle, D. Colson, and M. Viret, "Influence of parasitic phases on the properties of $BiFeO_3$ epitaxial thin films," Appl. Phys. Lett. **87**(7), 072508 (2005).
21. R. Nechache, C. Harnagea, L.-P. Carignan, O. Gautreau, L. Pintilie, M. P. Singh, D. Menard, P. Fournier, M. Alexe, and A. Pignolet, "Epitaxial thin films of the multiferroic double perovskite Bi_2FeCrO_6 grown on (100)-oriented $SrTiO_3$ substrates: growth, characterization, and optimization," J. Appl. Phys. **105**(6), 061621 (2009).
22. S. Fujino, M. Murakami, S. H. Lim, L. G. Salamanca-Riba, M. Wuttig, and I. Takeuchi, "Multiphase growth in Bi-Mn-O thin films," J. Appl. Phys. **101**(1), 013903 (2007).
23. A. Sharan, J. Lettieri, Y. Jia, W. Tian, X. Pan, D. G. Schlom, and V. Gopalan, "Bismuth manganite: A multiferroic with a large nonlinear optical response," Phys. Rev. B **69**(21), 214109 (2004).
24. J. F. Scott, "Ferroelectrics go bananas," J. Phys. Condens. Matter **20**(2), 021001 (2008).
25. L. Pintilie and M. Alexe, "Ferroelectric-like hysteresis loop in nonferroelectric systems," Appl. Phys. Lett. **87**(11), 112903 (2005).
26. H. Kliem and B. Martin, "Pseudo-ferroelectric properties by space charge polarization," J. Phys. Condens. Matter **20**(32), 321001 (2008).
27. A. Loidl, S. Krohns, J. Hemberger, and P. Lunkenheimer, "Bananas go paraelectric," J. Phys. Condens. Matter **20**(19), 191001 (2008).
28. X. S. Xu, J. F. Ihlefeld, J. H. Lee, O. K. Ezekoye, E. Vlahos, R. Ramesh, V. Gopalan, X. Q. Pan, D. G. Schlom, and J. L. Musfeldt, "Tunable band gap in $Bi(Fe_{1-x}Mn_x)O_3$ films," Appl. Phys. Lett. **96**(19), 192901 (2010).
29. D. P. Dubal, D. S. Dhawale, R. R. Salunkhe, S. M. Pawar, V. J. Fulari, and C. D. Lokhande, "A novel chemical synthesis of interlocked cubes of hausmannite Mn_3O_4 thin films for supercapacitor application," J. Alloy. Comp. **484**(1), 218–221 (2009).
30. H. Y. Xu, S. L. Xu, X. D. Li, H. Wang, and H. Yan, "Chemical bath deposition of hausmannite Mn_3O_4 thin films," Appl. Surf. Sci. **252**(12), 4091–4096 (2006).
31. M. A. Quijada, J. R. Simpson, L. Vasiliu-Doloc, J. W. Lynn, H. D. Drew, Y. M. Mukovskii, and S. G. Karabashev, "Temperature dependence of low-lying electronic excitations of $LaMnO_3$," Phys. Rev. B **64**(22), 224426 (2001).
32. N. N. Kovaleva, A. V. Boris, C. Bernhard, A. Kulakov, A. Pimenov, A. M. Balbashov, G. Khaliullin, and B. Keimer, "Spin-Controlled Mott-Hubbard bands in $LaMnO_3$ Probed by Optical Ellipsometry," Phys. Rev. Lett. **93**(14), 147204 (2004).
33. A. S. Moskvin, A. A. Makhnev, L. V. Nomerovannaya, N. N. Loshkareva, and A. M. Balbashov, "Interplay of p-d and d-d charge transfer transitions in rare-earth perovskite manganites," Phys. Rev. B **82**(3), 035106 (2010).
34. J. Wei, D. Xue, C. Wu, and Z. Li, "Enhanced ferromagnetic properties of multiferroic $Bi_{1-x}Sr_xMn_{0.2}Fe_{0.8}O_3$ synthesized by sol–gel process," J. Alloy. Comp. **453**(1–2), 20–23 (2008).
35. C. F. Chung, J. P. Lin, and J. M. Wu, "Influence of Mn and Nb dopants on electric properties of chemical-solution-deposited $BiFeO_3$ films," Appl. Phys. Lett. **88**(24), 242909 (2006).
36. V. K. Yarmarkin, B. M. Gol'tsman, M. M. Kazanin, and V. V. Lemanov, "Barrier Photovoltaic Effects in PZT Ferroelectric Thin Films," Phys. Solid State **42**(3), 522–527 (2000).
37. A. Matsumura, Y. Kamaike, T. Horiuchi, M. Shimuzi, T. Shiosaki, and K. Matsushige, "Thermal Effects in Properties of Photovoltaic Currents of Pb(Zr, Ti)O_3 Thin Films," Jpn. J. Appl. Phys. **34**(9B), 5258–5262 (1995).
38. H. Yang, H. M. Luo, H. Wang, I. O. Usov, N. A. Suvorova, M. Jain, D. M. Feldmann, P. C. Dowden, R. F. DePaula, and Q. X. Jia, "Rectifying current-voltage characteristics of $BiFeO_3$/Nb-doped $SrTiO_3$ heterojunction," Appl. Phys. Lett. **92**(10), 102113 (2008).
39. Z. Yue, K. Zhao, S. Zhao, Z. Lu, X. Li, H. Ni, and A. Wang, "Thickness-dependent photovoltaic effects in miscut Nb-doped $SrTiO_3$ single crystals," J. Phys. D Appl. Phys. **43**(1), 015104 (2010).
40. Y. Muraoka, T. Muramatsu, J. Yamaura, and Z. Hiroi, "Photogenerated hole carrier injection to $YBa_2Cu_3O_7$−x in an oxide heterostructure," Appl. Phys. Lett. **85**(14), 2950–2952 (2004).
41. F. Horikiri, T. Ichikawa, A. Kaimai, H. Matsumoto, K. Yashiro, T. Kawada, and J. Mizusaki, "High temperature photovoltaic effect at Nb doped $SrTiO_3$/electrode," *http://www.electrochem.org/dl/ma/206/pdfs/1783.pdf*
42. Y. J. Hwang, A. Boukai, and P. Yang, "High density n-Si/n-TiO_2 core/shell nanowire arrays with enhanced photoactivity," Nano Lett. **9**(1), 410–415 (2009).
43. Y. Watanabe, "Electrical transport through Pb(Zr,Ti)O_3 p-n and p-p heterostructures modulated by bound charges at a ferroelectric surface: ferroelectric p-n diode," Phys. Rev. B **59**(17), 11257–11266 (1999).
44. R. Meyer and R. Waser, "Hysteretic resistance concepts in ferroelectric thin films," J. Appl. Phys. **100**(5), 051611 (2006).

#195123 - $15.00 USD Received 2 Aug 2013; revised 25 Nov 2013; accepted 25 Nov 2013; published 5 Dec 2013

1. Introduction

In photovoltaic devices, photons with energy higher than the band gap of the material are absorbed to create excitons. The latter are then separated by an internal electric field and collected by the electrodes. The efficiency of charge carrier collection therefore depends on the magnitude of the internal electric field present inside the material. This field usually originates from a p-n homo or hetero-junction [1] that forms depending on the nature of semiconductor material used in the device. To effectively collect the photo carriers in this scenario, the contacts between the electrodes and the semiconductor need to be ohmic. On the other hand, if the semiconductor-electrode interface creates a Schottky barrier [1], the latter could also contribute to the separation of the photo generated carriers. However, in ferroelectric materials, which possess a spontaneous polarization, there is an internal electric field (commonly identified with the depolarization field, E_{DP}) that extends over the whole thin film volume [2,3], thereby separating the charge carriers even more efficiently. In contrast to the case of a p-n junction or that of a metal-insulator junction interface, where only the depletion region takes part in the photo carrier separation process, the depolarization field present in ferroelectric materials drives the photo carriers towards electrodes. Recently, the combined effect of the electrical properties of normal *p-n* junctions, semiconductor-metal interfaces and the exotic properties of ferroelectric oxides have been the subject of intensive theoretical and experimental studies [4–6]. To date, the photovoltaic properties of several ferroelectric oxides have been investigated including $BaTiO_3$ (BTO), $Pb(Zr,Ti)O_3$ (PZT) and BFO [7–10]. However, the photovoltaic devices built using these materials exhibited a very low power conversion efficiency, typically of the order of 10^{-7}-10^{-5}, primarily due to the relatively large band gap and insulating properties of typical ferroelectrics.

Multiferroic (MF) perovskites have been studied extensively during the last decade, mainly driven by the exciting phenomena that occur due to the co-existence of ferroelectricity and magnetism in a single phase, among which is the decrease of the band gap [11]. The small bandgap of MF materials (typically ranging from 1.1 eV to 2.7 eV) is an essential key parameter in terms of PV research, since about 93% of solar radiation is concentrated in the visible and infrared light with a wavelength corresponding to photon energies in the range of 0.31–3.18 eV) [12]. So far, the most widely investigated MF material for such applications is $BiFeO_3$ (BFO) [13,14].

Among known MFs, $BiMnO_3$ (BMO) is the most "fundamental" one, being referred to as the "hydrogen atom" of multiferroic materials [15]. The crystal structure of BMO films belongs, at room temperature, to the monoclinic C2 space group with the following lattice parameters: a = 9.523 Å, b = 5.6064 Å, and c = 9.8536 Å, $\alpha = \gamma = 90°$, and $\beta = 110.667°$. BMO exhibits the lowest bandgap (typically 1.2 eV) and a ferroelectric spontaneous polarization of up to 16 $\mu C/cm^2$ in thin film form [16]. The low band gap of ferroelectric BMO films results in greater light absorption and reduced photo charge recombination, both of which are critical issues for improving PV efficiency. Combination of bulk PV effect originated from ferroelectric polarization and film/electrodes interfacial effect of BMO thin films would further enhance PV performance of the device. The ferroelectric properties of the films however, depend on the optimized growth condition [17,18] as well as on device architecture, which has to be optimized to reduce leakage currents in BMO films [16]. The growth conditions, crystal structure and quality of the as prepared BMO films are the most fundamental parameters for tuning functional properties.

Here we report the observation of the PV effect of heterostructures based on BMO thin films. We describe the PV phenomena in terms of the film/substrate hetero-structure interface that could be modulated by the effect of polarization induced internal electric field. BMO thin films were grown on (111)-oriented niobium doped $SrTiO_3$ (STO:Nb) substrates by pulsed lased deposition (PLD). The Bi/Mn ratio was tuned by varying PLD deposition parameters to study its effect on the physical properties of the films. The films crystallize in two phases: perovskite BMO (major component) and Mn_3O_4 (MO) (minor phase). Both phases exhibit epitaxial order on STO. The PV effect observed in the films is found to be strongly dependent

#195123 - $15.00 USD Received 2 Aug 2013; revised 25 Nov 2013; accepted 25 Nov 2013; published 5 Dec 2013

on the Bi/Mn ratio by both electrical and optical studies. The results demonstrate that an increased percentage of BMO phase in the films contributes significantly to the enhancement of the PV efficiency.

2. Experimental methods and results

The 70 nm thick films were grown by PLD using a BMO target with stoichiometric composition. According to the chemical formula of BMO, appropriate amounts of Bi_2O_3 and Mn_2O_3 oxides were ball-milled, dried and sintered to synthesize the target for PLD [19]. Before deposition, the PLD chamber was pumped to a vacuum level of $1x10^{-5}$ mbar. The laser fluence and pulse frequency were set at ~2.0 J /cm^2 and 4 Hz, respectively and we studied the effect of the substrate temperature and oxygen pressure during growth, when varied in the ranges 595–670 °C and 25–40 mTorr, respectively. The films were characterized using energy dispersive spectrometry (EDX) in a scanning electron microscope (SEM). We found that the Bi/Mn atomic ratio is clearly sensitive to deposition temperature and oxygen pressure, mainly due to the high volatility of elemental Bi. We identified three types of films (labeled A-C summarized in Table 1) together with deposition conditions and phases observed in the films. The table also reports the energy threshold for optical absorption extracted from optical measurements.

Table 1. Phases, Compositions and Optical Properties of Bi-Mn-O Films Grown by PLD on (111)-oriented Nb Doped $SrTiO_3$ Substrates

Film #	Deposition temperature (°C) & pressure (mTorr)	Bi/Mn ratio (at. %)	Phases	Energy threshold (eV)
A	595, 25	0.82	$BiMnO_3/Mn_3O_4$	1.2
B	670, 40	0.56	$BiMnO_3/Mn_3O_4$	1.5/2.2
C	670, 25	0.14	$BiMnO_3/Mn_3O_4$	2.6

Near-stoichiometric composition can only be achieved by growing at low temperature (Film type A- 595 °C) whereas a higher deposition temperature (e.g. 670 °C) yields manganese-rich films (Film type C). Increasing the flow of oxygen at higher deposition temperature (from 25 to 40 mTorr) minimizes Mn or increases Bi in the film (Film type B). Bi deficiency is due to its evaporation at high temperature, since this element is highly volatile. These results are consistent with several previous reports on other Bi-based perovskite systems [20,21].

Figure 1(a) displays x-ray diffraction (XRD) spectra (PANalyticalX'Pert Pro MRD 4-circle diffractometer system) of the obtained films which evidence their bi-phase character. The θ-2θ scans [Fig. 1(a)] reveal the preferential monoclinic $(11\text{-}1)_m$ orientation of the BMO phase following the cubic $(111)_c$ direction of the STO substrate. They also indicate the presence of an additional phase in all synthesized films, identified as Mn_3O_4. This phase exhibits a preferential orientation along the tetragonal $(101)_t$ direction. Phi (Φ) scan measurements around the STO (110) reflection confirm the epitaxial growth of BMO and Mn oxide phases on STO:Nb substrates with threefold symmetry [Fig. 1(b)]. The orientation relationships are as follows: $BiMnO_3$ (110)pc//$SrTiO_3$ (110)c//Mn3O4 (110)pc. A similar multiphase epitaxial growth was previously reported by Fujino et. al. in [22].

#195123 - $15.00 USD Received 2 Aug 2013; revised 25 Nov 2013; accepted 25 Nov 2013; published 5 Dec 2013

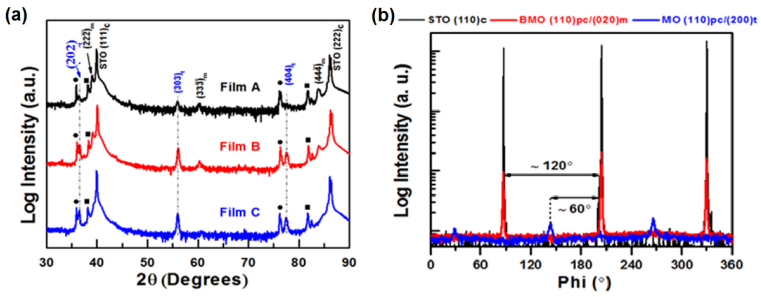

Fig. 1. (a) XRD θ-2θ scans of the three types of films grown on (111) oriented STO: Nb substrate, showing the reflections of the $(11\text{-}1)_m$ orientation of BMO and that of the $(101)_t$ orientation of Mn_3O_4 phase. Circular and rectangular symbols in (a) indicate (00l) K_β lines and tungsten contamination of the x-ray tube source. (b) Φ scan measurements show the three fold symmetry of BMO and Mn oxide phases in the films.

To perform electrical measurements, 2D arrays of Indium Tin Oxide (ITO) top electrodes were deposited by PLD through a shadow mask, at 200 °C under 10 mTorr oxygen partial pressure. Electrical measurements were performed by applying a bias voltage between the ITO top electrodes and the doped STO substrate, which acts as a bottom electrode.

Figure 2 illustrates Current density-Voltage (J-V) curves (measured by computer controlled Keithley 2400 Digital Source Meter) of two films measured under both dark and 1.5 AM sun (100 mW/cm^2) illumination using SS50AAA solar simulator, class AAA. Figure 2(a) and 2(b) (J-V plotting of olive green color) displays the dark current and PV effect of the as-grown Film type A. The samples were subsequently electrically poled by applying 1 microsecond voltage pulses of - 10 or + 10 V between the top and bottom electrodes. This procedure was performed so as to orient the ferroelectric polarization "up" or "down" along the direction normal to the film plane, where "up" corresponds to an orientation from the STO substrate to the top electrode [23]. Since we found a significant PV effect only in films types A & B, the data from Film type C is not shown.

Figure 2(b) and 2(d) shows the change of the J-V curve obtained after applying alternating voltage pulses, inducing the reversal of the direction of polarization in the films. The dark current measurements reported in Fig. 2(d) were obtained after downward poling. Film type A yields V_{oc}~0.56 V and J_{sc}~0.23 mA/cm^2, whereas lower values, respectively whereas 0.22 V and 0.11 mA/cm^2 were recorded for Film type B. The calculated maximum power conversion efficiency, PCEs in Films A and B are 0.1% and 0.01%, respectively. Likewise, the fill factor (FF) for Film type A is higher (~0.71) than the one of Film type B (~0.47) [calculated as FF = $P_{out}^{max}/(V_{oc}*J_{sc})$]. These results demonstrate that films with a higher Bi/Mn ratio generate a higher power conversion efficiency.

The switching behavior of the macroscopic polarization by TFA Analyzer 2000 is shown in Fig. 3(a), for Films types A & B (without illumination). We found a remnant polarization of 6.6 μC/cm^2 for film type A and 5.5 μC/cm^2 for film type B, values far below the one reported for BMO film [16]. The loops are well-saturated at negative bias (polarization up) and show a significant leakage contribution on the positive side, consistent with the J-V curves in Fig. 2. The hysteresis loop of Film type B shows a more pronounced leaky character, probably due to a larger density of interphase boundaries that imply a higher density of defects, but the existence of a switchable ferroelectric polarization is certain, as demonstrated by measurements at different cycling frequencies, see in Fig. 5.

#195123 - $15.00 USD Received 2 Aug 2013; revised 25 Nov 2013; accepted 25 Nov 2013; published 5 Dec 2013

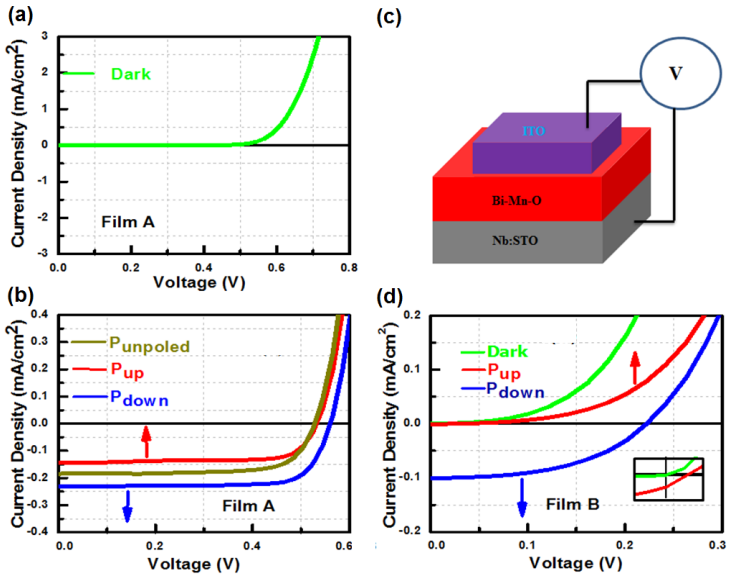

Fig. 2. J-V characteristic curves of Film A (a) & (b), and Film B (d) respectively, with positive and negative poling demonstrating the photovoltaic (PV) effect. The inset in (d) represents a zoom of the J-V curve around origin. The geometry of the tested structure is illustrated in (c).

The fact that the hysteresis loop parameters do not change significantly when modifying the cycling frequency by a factor of 20 prove that the measured charge flow originates in their switching of polarization and is not due to other effects [24–27]. Beside the leakage, another important property that can be extracted from the ferroelectric loops is the imprint of polarization. As observed in Fig. 3(a), the positive coercive voltage is higher than the negative one and the fact that polarization requires a higher voltage to switch downward implies that there is an internal built-in field opposing this process. This net field oriented upward has a major contribution to the charge separation, as we shall discuss below. At the same time, in the film/STO interface region polarization is pinned downwards most likely due to the internal stresses caused by the lattice mismatch. This imprint of polarization was confirmed by piezoresponse force microscopy, see in Fig. 6.

We then performed optical measurements to study the absorption properties of each film. To investigate the optical absorption properties of epitaxial films, room temperature ellipsometry measurements (J.A. Woollam Company) were performed in the range of 1.25 to 3.35 eV at five angles of incidence (i.e. 55, 60, 65, 70 and 75°). The absorption coefficients $\alpha = 4\pi k/\lambda$ (where k and λ denote the extinction coefficient and wavelength, respectively) estimated for the different films are presented as a function of photon energy $E < 3.5$ eV in Fig. 3(b).

By increasing the BMO phase in the films, the 2.0 eV charge gap (Film C) broadens, begins to redshift and eventually develops into the 1.6 eV band in Film A [cf. Fig. 3(c)]. Plots of $(\alpha E)^2$ versus photon energy place the band gap in Film type A and Film type C at ~1.1 and 2.3 eV, respectively [cf. Fig. 3(c)]. These values are close to the ones previously observed in BMO films [28] and the well-documented Mn_3O_4 [29,30]. In the BMO case, comparing with theoretical and experimental spectra of chemically similar materials, like $LaMnO_3$ [31,32], where Mn^{3+} centers are in locally distorted octahedra at the near infrared band of 1.6-1.9 eV (with an overall intensity α around 10^5 cm^{-1}), this peak is assigned to the complex combination between O 2*p* and Mn 3*d* states (p-d) charge transfer excitations and inter-site $d(e_g)$-$d(e_g)$ high spin charge transfer (HSCT) transitions [33]. The particular shape of $(\alpha E)^2$ plot obtained for Film type B, where two linear parts (i.e. 1.1 and 2.2 eV) are distinguished, clearly indicates that the optical properties of our BMO thin films are a superposition of spectral responses of BMO and Mn oxide.

#195123 - $15.00 USD Received 2 Aug 2013; revised 25 Nov 2013; accepted 25 Nov 2013; published 5 Dec 2013

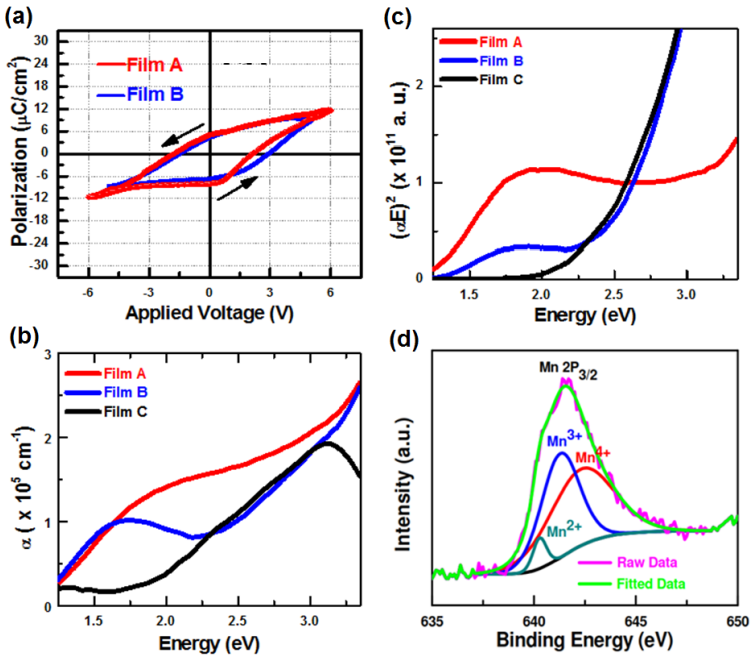

Fig. 3. (a) Macroscopic ferroelectric hysteresis obtained from Film A and Film B (a) Optical absorption coefficient (α) curves as a function of photon energy, measured by Ellipsometry for multiphase Bi-Mn-O thin films (c) corresponding estimated indirect bandgaps (d) Deconvoluted XPS spectra of the Mn $2p_{3/2}$ peak.

The electronic and chemical properties of Film type A were analyzed by X-ray photoelectron spectroscopy (XPS) (XPS-ESCA Escalab 220iXL). Figure 3(d) exhibits the Mn $2p_{3/2}$ peak spectrum of Film A. The peak is deconvoluted and compared with the corresponding peaks of Mn^{2+}, Mn^{3+} and Mn^{4+} valence states having a binding energy of 641 eV, 641.66 eV and 642.75 eV respectively [34,35]. The curve fittings for the high resolution peaks were determined using a least-squares method using Gauss-Lorentz function with a Shirley background subtraction [21]. Comparing the area under each curve, we conclude that Mn^{3+} is the highest valence state in this film which is correlated with charge transfer in the optical absorption spectra.

3. Analysis of results

The non-zero photovoltage and photocurrent observed in Film type A (unpoled state) can be described in terms of the interfacial effect i.e. interface PV phenomena [36,37]. In this model, we neglect the ferroelectric effect in the unpoled films. We neglect the Mn oxide phase in the film for PV effect analysis because of the presence of higher percentage (~85% with ~2% error) of $BiMnO_3$ phase in Film type A. The percentage of two phases has been estimated by taking into account the Bi/Mn atomic ratio measured in EDS-SEM (Table 1). Neglecting the MO phase is justified by the fact that Film type C, which contains a higher percentage of the MO phase, does not harvest any significant electricity. We then performed Ultra violet photoemission spectroscopy (UPS) measurements on the BMO films, to determine the position of the valence band energy (E_V) and Fermi energy (E_F). Taking into account the band gap of the BMO phase (~1.1 eV), we calculated the electron affinity of Film A from the following equation: $\chi = h\gamma - W - E_g$ where 'W' and 'hγ' (21.2 eV) denotes the width of the photoemission spectrum and excitation energy respectively. The calculated electron affinity is ~3.03 eV ± 0.2. The resulting band diagram of the ITO/BMO/STO heterostructure before and after its formation is shown in Fig. 4. The electron affinity and band gap of doped STO were obtained from reference [38], for the given dopant concentration of 1wt%. In this diagram we

#195123 - $15.00 USD Received 2 Aug 2013; revised 25 Nov 2013; accepted 25 Nov 2013; published 5 Dec 2013

assumed an ideal interface, where the charge traps at the film/electrode interfaces are neglected [1]. Figure 4(a) shows the position of the E_F slightly below the middle of the band gap which implies that the film exhibits a p-type conduction, probably caused by a low amount of Bi vacancies, as is often the case for Bi-based perovskites thin films due to the high volatility of Bi. Nonetheless, many reports described that Nb doped STO is able to generate excitons under illumination and acts as a n-type material [39–41]. Thus, in our heterostructure, the net effect of the formation of both a p-n junction and a Schottky junction at the film/substrate interface and film/top electrode, is an electric field oriented upward, which separates the photo generated charge carriers. The theoretically calculated net internal potential is $\Delta\Phi_{B\_ITO/BMO/Nb:STO} = 0.62$ eV. The actual photovoltage is slightly lower because of surface states at both interfaces that reflects in our experimentally yielded photovoltage (V_{OC}) in the unpoled state in Fig. 2. Figure 4(b) illustrates the possible charge flow in the film/STO substrate interface under illumination. The bend bending at film/STO interface shown here is assumed to be very similar to that of a TiO_2/Si contact in a photo electrochemical cell [42]. The e^-/h^+ pairs are generated in both film and STO. Under illumination, electron transfer starts to set up in the junction due to the difference of quasi Fermi energy level of electrons and holes in film and STO. The photogenerated electrons in the film are directed towards the ITO/film interface due to the internal built-in field established at the film/substrate junction. Photo generated holes recombine with a fraction of electrons in the conduction band of STO. This recombination at the junction reduces the loss of holes in the STO thus increasing the photocurrent. However, Fig. 4(c) shows the overall band bending, where the Schottky field is higher and oppositely directed with respect to the field set up at the BMO/STO interface. Therefore, the net electron flow will be from top to the bottom electrode due to the effect of the net electric field, in good agreement with the J-V curve and with the imprint of polarization inferred from the hysteresis loops. The whole mechanism is illustrated schematically in Fig. 4(c).

The tunability of the J-V curve can be described by taking into consideration the ferroelectric polarization. Depending on the direction of the switchable ferroelectric polarization, aggregated bound charges at the interface of the p-n junction might penetrate (decrease or increase) the depletion width and height of potential barrier, an effect called polarization modulation effect [43,44]. This modulation effect can explain the tunability of the J-V curve in Fig. 2.

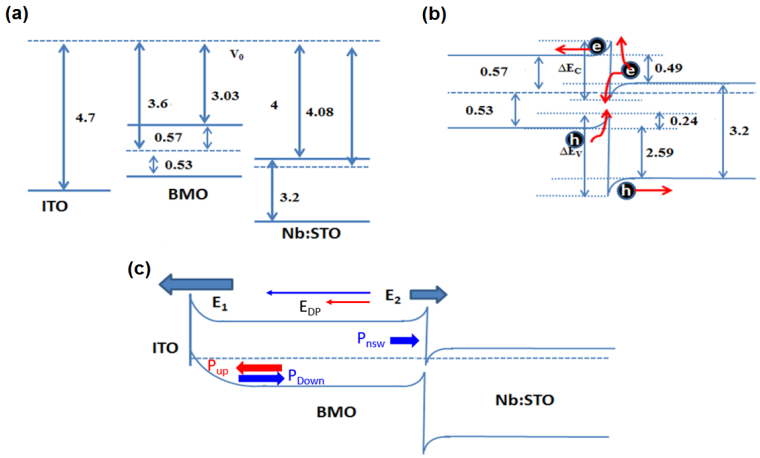

Fig. 4. (a) Energy band diagram of isolated ITO, BMO and doped STO (b) Energy band diagram of an ideal BMO/Nb:STO interface at thermal equilibrium **(c)** Energy band diagram of ITO/BMO/Nb:STO interface with showing the polarization effect. All units are in eV.

As shown in Fig. 4, there are two parts of the ferroelectric polarization: non switchable polarization (P_{nsw}), which originates from the compressive strain in the film (polarization pinning at the film/electrode interface) and switchable polarization (P_{sw}). Elaborately, the

#195123 - $15.00 USD Received 2 Aug 2013; revised 25 Nov 2013; accepted 25 Nov 2013; published 5 Dec 2013

depolarization field associated with P_{down} oriented towards the bottom electrode (the same direction as P_{nsw}) increases the barrier height at the film/ITO interface. Therefore, the photocurrent will be higher in this case, as shown in Fig. 2(b). The opposite direction of polarization P_{up} decreases the barrier height at the film/ITO interface, resulting in a small reduction of the photocurrent density compared to the unpoled condition. However, the estimation of the electric field at each interface and the estimation of polarization induced electric field could give the contribution of each on observed photocurrent and photovoltage. Individual contribution may help to elucidate which one dominates the current flow. This will be the subject of a future investigation.

4. Conclusion

We report the PV properties of epitaxial BMO-MO films on (111)-oriented Niobium doped STO substrates. We found an external power conversion efficiency of ~0.1% in the Film A when illuminated under sun simulator (AM 1.5G). Our results show that the photocurrent and photo voltage strongly depends on the Bi/Mn ratio in the film, with the best power conversion efficiency being obtained in films with a high Bi/Mn ratio and thus a high BMO content. We used a traditional interfacial model (interface generated electric field) to explain the photovoltaic effect, that is significantly affected by the spontaneous polarization. Further studies are needed in order to understand and elucidate the complex interplay between the metal-ferroelectric interface and ferroelectric polarization involved in such device architecture.

Appendix

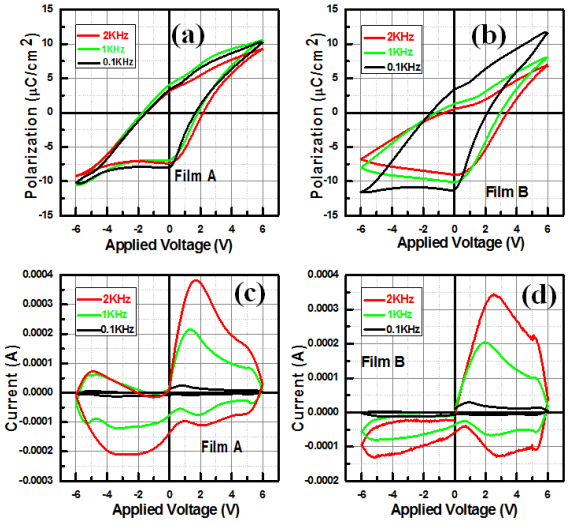

Fig. 5. Ferroelectric hysteresis loops (a, b) and the corresponding current loops (c, d) at different cycling frequencies: while there is a significant leakage contribution, the fact that the switching current dominates at low frequency proves the existence of the ferroelectric component.

#195123 - $15.00 USD Received 2 Aug 2013; revised 25 Nov 2013; accepted 25 Nov 2013; published 5 Dec 2013

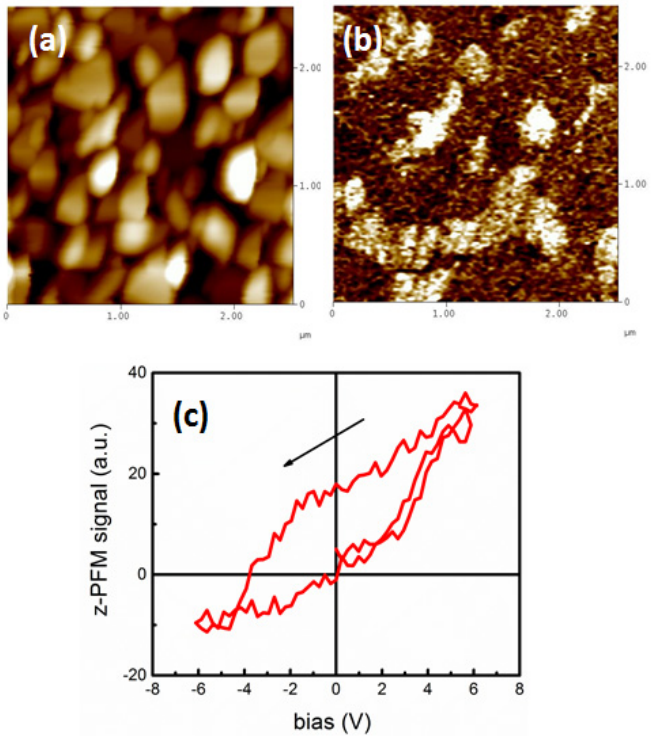

Fig. 6. Piezoresponse force microscopy measurement showing that the as-grown epitaxial BMO/STO(111) heterostructure has the polarization oriented downward (bright contrast). (a) surface topography, and (b) PFM image. The regions/grains that do not show a response (grey contrast) are either oriented in-plane, or represent the minor MO phase. (c) Out-of-plane PFM hysteresis loop obtained from one of the grains, showing the significant imprint of polarization.

Acknowledgments

We acknowledge infrastructure support from the Canada Foundation for Innovation. F.R. is grateful to the Canada Research Chairs Program for partial salary support. F.R. is also supported by FQRNT équipe (Quebec) projects and an NSERC Discovery Grant. F.R. acknowledges MDEIE (Quebec) for an international collaboration grant. R.N. is grateful to the NSERC PDF fellowship program (Canada) for partial salary support.